Annexin XII E105K Crystal Structure: Identification of a pH-Dependent Switch for Mutant Hexamerization†

J.-P. Cartailler,‡,§ H. T. Haigler,|| and H. Luecke*,‡,§,||

Department of Molecular Biology & Biochemistry, Program in Macromolecular Structure, and Department of Physiology and Biophysics, University of California, Irvine, California 92697-3900

Received September 30, 1999

ABSTRACT: Annexins are a family of calcium- and phospholipid-binding proteins involved with numerous cellular processes including membrane fusion, ion channel activity, and heterocomplex formation with other proteins. The annexin XII (ANXB12) crystal structure presented evidence that calcium mediates the formation of a hexamer through a novel intermolecular calcium-binding site [Luecke et al. (1995) *Nature 378*, 512−515]. In an attempt to disrupt hexamerization, we mutated a conserved key ligand in the intermolecular calcium-binding site, Glu105, to lysine. Despite its occurrence in a new spacegroup, the 1.93 Å resolution structure reveals a hexamer with the Lys105 ϵ-amino group nearly superimposable with the original intermolecular calcium position. Our analysis shows that the mutation is directly involved in stabilizing the hexamer. The local residues are reoriented to retain affinity between the two trimers via a pH-dependent switch residue, Glu76, which is now protonated, allowing it to form tandem hydrogen bonds with the backbone carbonyl and nitrogen atoms of Thr103 located across the trimer interface. The loss of the intermolecular calcium-binding site is recuperated by extensive hydrogen bonding favoring hexamer stabilization. The presence of this mutant structure provides further evidence for hexameric annexin XII, and possible in vivo roles are discussed.

Annexins are a family of Ca^{2+}/phospholipid-binding proteins which possess a canonical motif comprising of a stretch of approximately 70 amino acids, usually repeated 4 times, responsible for calcium-dependent phospholipid binding (review in ref *10*). A highly variable N-terminal domain, defined by its sequence and length, is believed to determine individual annexin functions (*24*). These tails share sequence similarity only at conserved phosphorylation sites for protein kinase C (PKC) and tyrosine kinases (*25*). Putative annexin functions include phospholipase A_2 inhibition (PL-A_2), cell proliferation/differentiation, membrane fusion/aggregation, exocytosis, PKC inhibition, and ion channel activity (*33*, *28*, *10*). It is evident that annexins mediate important cellular events, yet their unique functions are still being researched.

Hydra vulgaris annexin XII (ANXB12) has been shown to be a marker for hydra head regeneration, localized in the cytoplasm of ectodermal tentacle battery cells (*26*). Dramatic increases in annexin XII expression occur at the base of the tentacle in the newly formed battery cells (*26*), within the tentacle zone where the stimulus for the epithelial to battery cell differentiation event occurs (*6*). Annexin XII was found to be phosphorylated by an endogenous hydra protein kinase C in vitro (*27*). Since diacylglycerol (a PKC activator) will induce and influence the regenerating body column tissue into forming head structures, annexin XII phosphorylation may be involved in signal transduction events. Therefore, annexin XII expression in the newly formed battery cells may be intimately associated with or occurs as a direct result of the epithelial to battery cell differentiation process.

In crystals, annexins have been found as monomers (*36*), dimers (*18*), trimers (*4*, *31*), and hexamers (*19*). The annexin XII crystal structure revealed a homohexamer shaped like a double-concave disk about 100 Å in diameter and 70 Å thick with a prominent central funnel-shaped pore evident along the 3-fold axis. The annexin XII monomer fold is equivalent to that of annexins I (*36*) and V (*12*), but in addition contains six identical and novel intermolecular Ca^{2+} -binding sites that were proposed to mediate the formation of the homohexamer (*19*). Also present are the previously characterized type II Ca^{2+}-binding sites that are believed to mediate phospholipid binding, with three of these occupied by calcium in each monomer.

The type II calcium-binding site consensus sequence is usually G-X-G-T-(38)-D/E, formed by the AB/DE-loops. The calcium is typically coordinated by (i) 3 main chain carbonyl oxygen atoms in the AB-loop, (ii) a bidentate carboxylate group from an acidic side chain 38 residues downstream in sequence located within helix D, and (iii) water molecule(s). With more waters serving as ligands than high-affinity EF-hand calcium-binding sites, these type II sites are geometrically more flexible, allowing for interactions with acidic phospholipid headgroups. A "calcium-bridging" mechanism has been suggested to explain the tight, reversible membrane binding (*10*, *28*). A water molecule from the apical position of the coordination sphere is indeed replaced

† This work was supported by NIH Grants GM56445 (H.L.) and GM55651 (H.T.H.) and by an NIH Structural Biology Training Grant (J.-P.C.).

* Address correspondence to this author. E-mail: HUDEL@UCI.EDU.
‡ Department of Molecular Biology & Biochemistry.
§ Program in Macromolecular Structure.
|| Department of Physiology and Biophysics.

10.1021/bi992278d CCC: $19.00
Published on Web 02/19/2000

by a phosphoryl oxygen of the phospholipid backbone, allowing simultaneous calcium coordination between the protein ligands and polar moieties of phospholipid molecules, as shown by Swairjo and co-workers (*32*). Lower affinity type III binding sites have been observed in which calcium ions are bound to the DE-loop by one or two main chain carbonyl oxygens, a bidentate carboxylate from the E helix, and several water molecules as seen in the annexin I crystal structure (*36*).

The novel calcium-binding site discovered in the wild-type annexin XII hexamer is reminiscent of the type III calcium-binding site with the backbone carbonyl oxygens donated by Lys68 and Leu71 and the carboxylate by Glu76 of the domain 1 DE-loop. However, Glu76 is not bidentate to the calcium since its OE1 is accepting a hydrogen bonded from the backbone nitrogen of Thr103 in the opposing monomer. This adjacent monomer also contributes a glutamate (Glu105) carboxylate to this calcium to form a novel intermolecular calcium-binding site believed to mediate hexamer formation, occurring twice in each 'dimer'.

Investigation of the multimeric states of annexin XII has shown that the wild-type protein forms Ca^{2+}-dependent trimers/hexamers in solution (*20*) and trimers in the presence of bilayers (*16*), as determined by chemical cross-linking and by electron paramagnetic resonance (EPR), respectively. However, the EPR experiments, performed at lower calcium concentrations and in the absence of phospholipid vesicles, failed to detect trimer and hexamer formation in solution. Annexin V chemical cross-linking also showed calcium-dependent formation of trimers, hexamers, and higher aggregates in the presence of anionic phospholipids (*3*). Further evidence for annexin calcium-dependent self-association into higher oligomers, composed of 50 × 150 Å rods, was also shown for annexin VII (*5*).

In the present work, we decided to mutate the highly conserved glutamate 105 to lysine (E105K) with the aim of disrupting the intermolecular calcium-binding site of the wild-type hexamer by the introduction of a nonfavorable charge. As seen in the chemical cross-linking study by Maillard and co-workers (*20*), the E105K mutation disrupted the hexamerization event in solution. As revealed by nonactin conductance probe experiments, dramatic differences exist between the wild-type and E105K proteins with regard to their interaction with planar bilayers (unpublished experiments, with J. E. Hall, UCI). To investigate the basis of these altered properties, we solved and refined the crystal structure of the mutant E105K to a resolution of 1.93 Å.

MATERIALS AND METHODS

Subcloning, Mutagenesis, Expression, and Purification of Annexin XII. Subcloning of the *H. vulgaris* annexin XII gene and subsequent site-directed mutagenesis of the intermolecular Ca^{2+}-binding site converting Glu105 to Lys105 were done as previously described (*20*). Protein expression and purification were also performed according to ref *20*.

Crystallization and Data Collection. Crystals of the E105K mutant protein were grown at 4 °C by the hanging-drop vapor diffusion method. Protein (8 mg/mL) was mixed with an equal volume of precipitant containing 0.2 M ammonium acetate (Sigma), 0.1 M sodium citrate, pH 5.6 (Sigma), and 80% 2-methylpentanediol (Fluka), as based on the Crystal Screen condition 21 (Hampton Research). Crystals appeared after 4−5 days and grew within 10 days to a size of 0.2 × 0.2 × 0.5 mm. Crystals have $P2_12_12_1$ symmetry with unit cell dimensions of $a = 68.94$ Å, $b = 162.54$ Å, $c = 188.80$ Å. For data collection, crystals were cryo-cooled in nylon loops at 100 K. X-ray diffraction data to 1.9 Å resolution, consisting of 144 ($\Delta\varphi = 1.0°$) frames, were collected at the Stanford Synchrotron Radiation Laboratory (BL 7-1), processed, and reduced with the program DENZO/SCALEPACK (*23*), yielding a completeness of 92.5% and R_{sym} of 5.6%. Complete crystallographic statistics are shown in Table 1.

Table 1: Statistics for Data Collection and Refinement

spacegroup	$P2_12_12_1$
cell constants (Å)	$a = 68.94$, $b = 162.54$, $c = 188.80$
data collection resolution (Å)	1.90−25.0
reflections measured	969367
unique reflections	156877
mosaicity (deg)	0.42
R_{sym} (%),[a] overall	5.6
R_{sym} (%), 1.93−1.97 Å shell	28.3
average $I/\sigma(I)$	20.6
average $I/\sigma(I)$, 1.93−1.97 Å shell	3.6
completeness (%), overall	92.5
completeness (%), 1.93−1.97 Å	93.8
non-hydrogen protein atoms	14768
calcium atoms	11
solvent molecules	926
refinement resolution range (Å)	1.93−10.00
reflections used for refinement	155796
R-factor[b] (%) for data with $F > 4\sigma(F)$/all data	20.8/23.0
R_{free}[c] (%) for data with $F > 4\sigma(F)$/all data	26.3/28.7
rms standard deviations	
bond lengths (Å)	0.009
bond angles (deg)	1.5
average *B* value, protein (Å^2)	29.8
average *B* values, calcium (Å^2)	
domain II AB	51.8
domain III AB	39.8
average *B* values, waters (Å^2)	34.6

[a] $R_{sym} = [\Sigma_h\Sigma_i|(h,i) - \langle I(h)\rangle|/\Sigma_h\Sigma_i\ |(h,i)] \times 100$, where $I(h,i)$ is the intensity value of the ith measurement of h and $\langle I(h)\rangle$ is the corresponding mean value of h for all I measurements of h. The summation is over all measurements. [b] *R*-value $= (\Sigma|F_o - F_c|/\Sigma F_o) \times 100$. [c] R_{free} was calculated by randomly omitting 5% of the observed reflections from refinement and *R*-factor calculation (*2*).

Structure Determination. Since the mutant protein crystallized in a different spacegroup ($P2_12_12_1$) than the wild-type ($P2_1$), the structure was solved by molecular replacement. The V_M suggested six molecules in the asymmetric unit, and consequently the wild-type annexin XII hexamer (without calciums) was used as the search model. The solution yielded one hexamer in the asymmetric unit. X-PLOR (*2*) reported an initial crystallographic *R*-factor of 37.3% for data with an $F/\sigma(F) > 3$ between 2.5 and 10 Å which decreased to an *R*-factor of 20.4% and an R_{free} of 29.2% after 100 cycles of positional and *B*-factor refinement. This was followed by refinement with SHELXL-97 (*30*), applying 6-fold noncrystallographic symmetry (NCS) restraints for the entire model (including restraints for the NCS-related isotropic *B*-factors). More than 25 rounds of refinement and model building using the program O (*13*) were employed to rebuild loop regions and other areas. The types of maps used in model building were $3F_o - 2F_c$ and positive and negative $F_o - F_c$. Once the R_{free} had dropped below 30% [$F/\sigma(F) > 4$], water

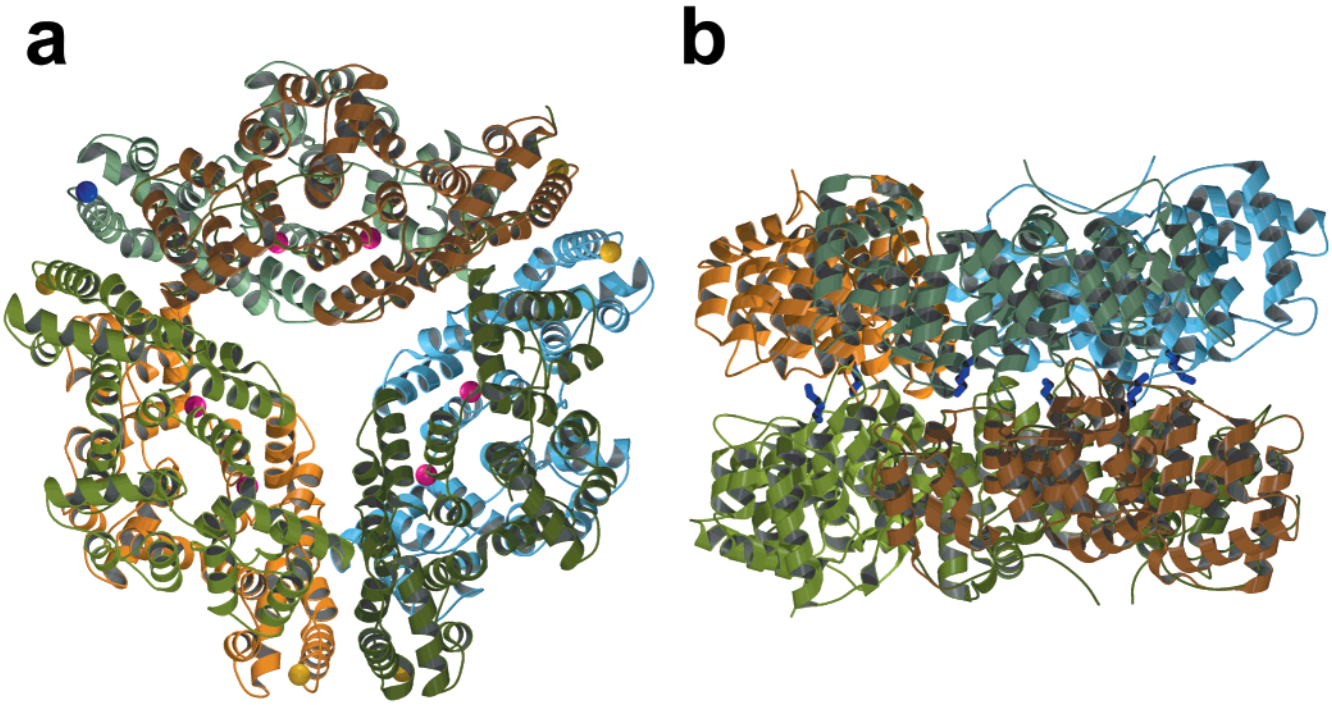

FIGURE 1: (a) Shown is the E105K hexamer viewed down the local 3-fold axis, with each subunit independently colored. The domain III type II calciums are shown in yellow for those modeled and blue for that absent. The domain II calcium-binding sites are shown in magenta. (b) Viewed from the side is the E105K mutation, repeated 6 times, represented by the blue stick model indicating its position at the convex interface between the trimers. Figures made with Molscript (*7*) and rendered with Raster3D v2.3 (*21*).

molecules were introduced into positive difference density. We found that removing NCS restraints from areas of flexibility did not aid in map interpretation or data statistics. Additionally, random displacement of atomic positions and *B*-values from their current value using MAIN (*34*, *35*) was utilized in the late stages of refinement in order to reduce model bias. The last round of model building involved using an omit map of all the calciums and remodeling these. The final model contains 14 768 non-hydrogen protein atoms, 11 bound calciums, and 926 waters. Using PROCHECK (*17*), we found that 97% of the residues are in the most allowed regions of the Ramachandran plot and the rest in the allowed regions. Other crystallographic statistics are shown in Table 1.

RESULTS

Overall Structure of E105K Annexin XII. The structure, with the E105K mutation, was obtained from crystals grown at pH 5.6 and at ambient (low) calcium concentration. Efforts to grow the mutant crystals in the same conditions as presented here but with varying calcium concentrations were unsuccessful. Despite our efforts to disrupt hexamerization by introducing the E105K mutation, the homohexameric quaternary structure (chains A−F) adopted by the mutant is essentially identical to the wild-type structure determined in the presence of 10 mM calcium: two trimers are joined at their convex faces containing the type II calcium-binding sites on their perimeters as shown in Figure 1. Each monomer consists of the four canonical domains, composed of five α-helices wound in a right-handed superhelix, arranged in a cyclic planar array. The complete N-terminal tail is well-resolved and hydrogen-bonded to the protein core. The PKC phosphorylation site, Thr6, is not solvent-exposed as its hydroxyl moiety is hydrogen-bonded to the main chain carbonyl oxygen of Ile313 as seen in the wild-type structure. We speculate that in order to become phosphorylated, the N-terminal must undergo a substantial conformational change to expose the PKC site. Electrostatic interactions and molecular surface complimentarity between two monomers of adjoining trimers (dimer across trimers) contribute to the formation of the hexamer. The intermolecular calcium-binding site in the wild-type structure consists mainly of two opposing negatively charged pockets stabilized by the divalent calcium cation. To our surprise, rather than disrupting this electrostatic attraction as intended, the ϵ-amino group of Lys105 forms hydrogen-bonding partners with atoms involved in coordination of the wild-type intermolecular calcium cation. The mutant protein loses six calcium coordination bonds and gains four hydrogen bonds, overall retaining the hexameric quaternary structure.

Based on the membrane-aggregating properties of annexins, it is conceivable that an alternate hexamer exists which is formed by two trimers coming together at their concave (N-terminal) sides, allowing the calcium-binding sites on the convex faces to interact optimally with the phospholipid headgroups of two different bilayers as shown in Figure 2. Indeed, this alternate hexamer exists in both the annexin XII wild-type and the E105K crystal forms. There is relatively little contact surface area between trimers for this conformation in both annexin XII crystal structures compared to the 20% buried surface area in the hexamer described here and previously (*19*). Interestingly, the few contacts along the crystallographic *a*-axis that exist between the trimers of the alternate hexamer are conserved in this new (E105K) crystal form as shown in Table 2. It is also noteworthy that the contacts between hexamers in the wild-type unit cell are predominantly hydrophobic whereas the mutant contacts are primarily polar.

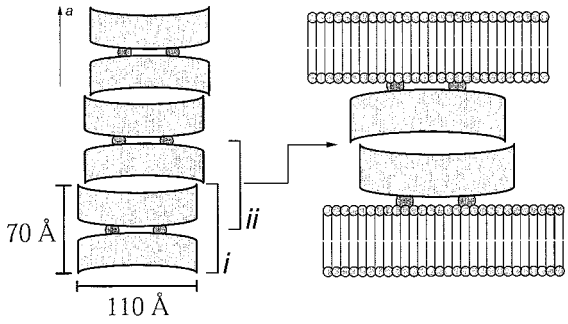

FIGURE 2: Shown is the crystallographic packing of the hexamer in both $P2_1$ (wild-type) and $P2_12_12_1$ (E105K) crystal forms along the crystallographic *a*-axis. Each concave disk represents one trimer, and the calciums are represented by gray circles. The hexamer is formed by tight, Ca^{2+}-mediated (wild-type) or pH-mediated (mutant) association of two convex faces (labeled *i*). The alternate hexamer which also exists in both crystal forms is comprised of two trimers interacting via their concave or N-terminal sides (labeled *ii*). The proposed model of bilayer aggregation by the alternate hexamer is also shown on the right where its calcium-binding sites associate with two independent bilayers.

Type II Calcium-Binding Sites. In the wild-type structure, which was crystallized at 10 mM calcium concentration, 18 peripheral type II calcium sites, proposed to be involved in phospholipid binding, are occupied in domains I, III, and IV. Surprisingly, the E105K mutant structure revealed that some of these sites were occupied, even though calcium was not added to the mother liquor during crystallization. Its presence must be attributed to it being carried over from the protein purification. The domain I AB-loop, consisting of residues 26−32, has uninterrupted main chain electron density but elevated *B*-factors (average of 54.0 Å^2). Difference electron density peaks indicated traces of solvent or calcium in these sites, but none were modeled due to the poor quality of the data in this region. It appears that the E105K mutation affects the nearby D-helix Glu70 geometry with respect to the AB-loop carbonyl ligands, therefore affecting the affinity of this site. Only five of the six domain III AB-loops (residues 180−187, with an average *B*-factor of 42.2 Å^2) are fully occupied by calcium ions with an average *B*-factor of 51.8 Å^2. A weak 2.5 σ difference density peak is present in the sixth (chain F) AB-loop, indicating partial occupancy of the site. Coupled with geometry indicative of calcium and not water, this was initially modeled as Ca^{2+}, but post-refinement indicated a high *B*-factor (over 100 Å^2) and was therefore removed from the model. Unlike the other subunits, the chain F Ile185 side chain is within van der Waals contact of a symmetry-related molecule, distorting and thus preventing this loop from adopting optimized coordination as observed from main-chain breaks in electron density. The domain IV calcium-binding loops (residues 257−262) were disordered throughout refinement with *B*-factors averaging 95.9 Å^2. Omit maps based on the final model failed to show any difference electron density, and this region was assigned zero occupancy. The average *B*-factor for all α-carbons is 29.8 Å^2, about 20 Å^2 higher than the wild-type 9.1 Å^2 and consistently so for most equivalent atoms as shown in Figure 3. The loop regions exhibit increased motion as expected from partial or lack of calcium occupancy.

Mixed Type II−III Calcium-Binding Site. The wild-type structure does not contain a type II binding site in domain II. The coordinating DE-loop glutamate 142 residue forms a salt-bridge with two lysine ϵ-amino groups, Lys99 from the same chain and Lys68 from the adjoining monomer (dimer across trimers), thereby sequestering it from coming into the coordination sphere for calcium binding. The 1.93 Å resolution E105K structure, in contrast to the wild-type 2.8 Å resolution, shows the presence of calcium in these loops, modeled late in refinement into 4.5σ difference density peaks. These calcium-binding sites are only partially occupied, as seen by elevated *B*-factors of the carbonyl ligands and calcium, and the calcium ions were modeled at 0.5 occupancy with an average *B*-factor of 39.8 Å^2. This difference does not appear to be related to local crystal-packing differences, as there are no packing contacts within 15 Å. We believe that the observation of these calciums may be due to two factors: (i) higher resolution data and (ii) the nearby mutation inducing small but significant changes in the positions of the main chain carbonyls, allowing for higher calcium affinity. The geometry consists of one or two backbone carbonyls from the AB-loop, with that from Met98 always present, and at least one water as shown in Figure 4. The glutamate "capping" residue is an average of 3.6 Å away from the calcium in an identical position as in the wild-type structure and therefore not within the calcium coordination sphere. Since this structure is a "low" calcium form, in contrast to the calcium-loaded wild-type structure, it is noteworthy that this site is even partially occupied while many sites that were fully occupied in the wild-type structure are now devoid of calcium.

The E105K Site. The glutamate to lysine mutation is located at the trimer−trimer interface as shown in Figure 1b. In the wild-type structure, the intermolecular calcium is coordinated by ligands from adjoining monomers (dimer across trimers). One monomer contributes Glu76-OE2 and the Lys-68 and Leu-71 backbone carbonyl oxygens, while the opposite monomer contributes Glu105-OE2 with a coordination distance of 2.19 ± 0.10 Å. It is likely that waters contribute to the coordination (i.e., between the more distant bidentate Asp230 and calcium), but none were modeled in the wild-type structure. The Glu76-OE1 is hydrogen-bonded to the Thr103 backbone nitrogen of the adjoining monomer. Each "local" dimer forms two sets of all of these interactions for a total of six. Hydrogen bonding and hydrophobic interactions supplement these in stabilizing the hexamer structure.

At first glance, the new E105K ϵ-amino group adopts the role of calcium. It is hydrogen-bonded to Asp230 of the same monomer and to the Lys68 and Leu71 backbone carbonyl oxygens of the opposite monomer. Glu76 of the opposite monomer, formerly a ligand in coordinating calcium, rotates to form a tandem hydrogen bond with the backbone Thr103 carbonyl oxygen and nitrogen of the adjacent monomer, with the new hydrogen bond between the protonated Glu76-OE2 and Thr103-C═O measuring 3.00 ± 0.21 Å. Furthermore, well-ordered water molecules near this site may further stabilize trimer−trimer interactions in the form of hydrogen bonds with shared ligands between these two as seen in Figure 5a. We expected, prior to the initial experiments, that the mutation would abolish hexamer formation as determined from chemical cross-linking studies. Yet, the hexamer persists and undergoes only minor structural rearrangements to retain

Table 2: Atomic Contacts between Symmetry-Related Hexamers for the E105K Mutant (Left Column) and Wild-Type (Right Column) Annexin XII[a]

E105K	central hexamer		symm. hexamer			WT	central hexamer		symm. hexamer		
sym (ABC)	residue	atom	residue	atom	interaction	sym (ABC)	residue	atom	residue	atom	interaction
1,0,0**	A Ala-11	CB	E Pro-164	CG	hydrophobic	1,0,0**	A Lys-8	NZ	E Asp-162	OD2	salt bridge*
	A Ala-167	N	F Asp-162	OD2	H-bond		A Ala-11	CB	E Pro-164	CG	hydrophobic
	A Ala-168	CB	F Pro-164	CB	hydrophobic		A Ala-167	N	F Asp-162	OD2	H-bond
	A Ala-168	N	F Asp-162	O	H-bond		A Ala-168	CB	F Pro-164	CG	hydrophobic
	B Pro-164	CG	D Ala-11	CB	hydrophobic		A Ala-168	N	F Asp-162	O	H-bond
	C Val-2	CG1/2	F Ala-11	CB	hydrophobic		B Asp-162	OD2	D Lys-8	NZ	salt-bridge*
	C Val-3	O	F Ser-12	OH	H-bond		B Pro-164	CG	D Ala-11	CB	hydrophobic
	C Ala-11	CB	F Val-2	CG1/2	hydrophobic		C Ala-11	CB	F Val-2	CG1/2	hydrophobic
	C Ser-12	OH	F Val-3	O	H-bond		C Asp-162	O	D Ala-168	N	H-bond
	C Asp-162	OD2	D Ala-167	N	H-bond		C Asp-162	OD2	D Ala-167	N	H-bond
	C Asp-162	O	D Ala-168	N	H-bond		C Pro-164	CG	D Ala-162	CB	hydrophobic
	C Pro-164	CG	D Ala-168	CB	hydrophobic						
-1,0,0**	D Ala-11	CB	B Pro-164	CD/CG	hydrophobic	-1,0,0**	D Lys-8	NZ	B Asp-162	OD2	salt-bridge*
	D Ala-167	N	C Asp-162	OD2	H-bond		D Ala-11	CB	B Pro-164	CG	hydrophobic
	D Ala-168	CB	C Pro-164	CG	hydrophobic		D Ala-167	N	C Asp-162	OD2	H-bond
	D Ala-168	N	C Asp162	O	H-bond		D Ala-168	N	C Asp-162	O	H-bond
	E Pro-164	CG	A Ala-11	CB	hydrophobic		D Ala-168	CB	C Pro-164	CG	hydrophobic
	F Val-2	CG1/2	C Ala-11	CB	hydrophobic		E Asp-162	OD2	A Lys-8	NZ	salt-bridge*
	F Val-3	O	C Ser-12	OH	H-bond		E Pro-164	CB	A Ala-11	CB	hydrophobic
	F Ala-11	CB	C Val-2	CG1/2	hydrophobic		F Val-2	CG1/2	C Ala-11	CB	hydrophobic
	F Ser-12	OH	C Val3	O	H-bond		F Asp-162	OD2	A Ala-167	N	H-bond
	F Asp-162	O	A Ala-168	N	H-bond		F Asp-162	O	A Ala-168	N	H-bond
	F Asp-162	OD2	A Ala-167	N	H-bond		F Pro-164	CG	A Ala-168	CB	hydrophobic
	F Pro-164	CB	A Ala-168	CB	hydrophobic						
0,0,1	A Asp-308	OD2	E Asn-216	OD1	H-bond	0,0,1	C Gly-259	N	B Ile-214	O	H-bond
	A Asp-308	OD1	E Asn-216	ND2	H-bond		C Leu-260	CD2	B Tyr-178	CE2	hydrophobic
0,1,1	B Tyr-295	OH	D Asn-216	ND2	H-bond		F Lys-258	CE	B Ile-185	CD1	hydrophobic
	B Glu-296	OE2	D Tyr-178	OH	H-bond		F Leu-260	CD1	B Tyr-178	CE2	hydrophobic
	B Asp-308	OD2	D Asn-216	OD1	H-bond		F Met-289	CB	E Ile185	CD1	hydrophobic
	B His-316	NE2	D Tyr-178	OH	H-bond		F Lys-297	CE2/CZ	B Ile-185	CD1	hydrophobic
-1,1,1	D Asn-216	ND2	B Tyr-295	OH	H-bond	0,0,-1	E Ile-185	CD1	F Met-289	CB	hydrophobic
	D Asn-216	OD1	B Asp-308	OD2	H-bond		B Glu-182	CA	C Leu-260	CD1/2	hydrophobic
	D Tyr-178	OH	B His-316	NE2	H-bond		B Ile-185	CD1	F Phe-297	CE2	hydrophobic
	D Tyr-178	OH	B Glu-296	OE2	H-bond		B Lys-213	CB/D	C Lys292	CD/E	hydrophobic
-1,0,1	E Asn-216	ND2	A Asp-308	OD1	H-bond		B Lys-213	CB/D	C Phe-297	CZ	hydrophobic
	E Asn-216	OD1	A Asp-308	OD2	H-bond		B Ile-214	O	C Gly-259	N	H-bond
2,1,0	C Thr-31	O	B Gln-221	NE2	H-bond	1,0,1	D Tyr-178	OH	E Trp-38	NE2	H-bond
	C Lys-34	NZ	B Asn-225	OD1	salt-bridge		D Ile-185	CG1	E Ala-11	CB	hydrophobic
	C Asp-305	OD1	B Asn-216	OD1	H-bond		D Asn-216	ND1	E Glu-17	OE2	H-bond
	F Glu-224	OE1	B His-209	ND1		1,-1,1	E Ala-11	CB	D Ile-185	CG1	hydrophobic
	F Asn-225	OD1	B His-205	NE2			E Glu-17	OE2	D Asn-216	OD1	H-bond
	F Ile-185	CG1	B Thr-285	CG2	hydrophobic		E Thr-21	OH	D Asn-216	ND2	H-bond
2,0,1	C Tyr-178	OH	F Glu-172	OE1	H-bond		E His-38	NE2	D Tyr-178	OH	H-bond
	C Ile-214	O	F His-169	NE2	H-bond	2,0,1	C Lys-213	O	E Leu-260	N	H-bond
	C Lys-217	NZ	E Glu17	OE1/2	salt-bridge		C Lys-213	NZ	E Cys-302	O	hydrophobic
	C Asn-216	OD1	E Asn-14	ND2	H-bond	2,-1,1	A Gly-259	N	C Ile-214	O	H-bond
	C Gln-221	OE1	E Ser-12	OH	H-bond		A Leu-260	N	C Lys-213	O	H-bond
	C Gln-221	NE2	E Ala-11	O	H-bond		A Leu-260	CD/CG	C Lys-213	CD1/2	hydrophobic
	F Ala-299	O	E Asp-300	OD2	H-bond		E Cys-302	O	C Lys-213	NZ	H-bond
	F Lys-307	NZ	E Asp-300	OD1	salt-bridge						
2,1,-1	B His-205	NE2	F Asn225	OE2	salt-bridge						
	B His-209	ND1	F Glu-225	OD1	salt-bridge						
	B Asn-216	O	C Glu-33	OE1/2	H-bond						
	B Asn-216	OD1	C Asp-305	OD1	H-bond						
	B Glu-221	NE2	C Thr-31	O	H-bond						
	B Asn-225	OD1	C Lys-34	NZ	salt-bridge						
	B Ala-288	CB	F Ile-185	CB	hydrophobic						
3,0,1	C Asn-206	NE2	A Asn-216	OE1	H-bond						
	C His-209	ND1	A Asn-216	OE1	H-bond						
	C His-209	NE2	A Ser-215	OE1	H-bond						
3,-1,1	A Asn-216	OD1	C Gln-206	NE2	H-bond						
	A Asn-216	OD1	C His-209	ND1	salt-bridge						
	A Ser-215	OD1	C His-209	NE2	H-bond						

[a] The central hexamer is displaced along the unit cell *a*, *b*, and *c* axes as indicated by the sym(ABC) column. We used XPAND (*14*) to generate all symmetry-related atoms whose distance to the surface of the "central" hexamer was less than or equal to 5 Å which were then imported into O for viewing. Hydrogen-bonding distances noted here were within 3.5 Å, and hydrophobic forces were cut off at 5 Å. The darkened cells represent common intermolecular contacts along the *a*-axis between each hexamer. Note: *The geometries for these are weak and are included only because these are not at all present in the mutant structure. **The 1,0,0 and −1,0,0 operators define the contacts of the alternate hexamer formed between the concave sides containing the N-terminals along the *a*-axis. These are the only ones to be overall conserved among the two crystal forms with some degree of variation. The packing contacts along the *b*,*c* axes are quite different between the wild type ($P2_1$) and mutant ($P2_12_12_1$) structures.

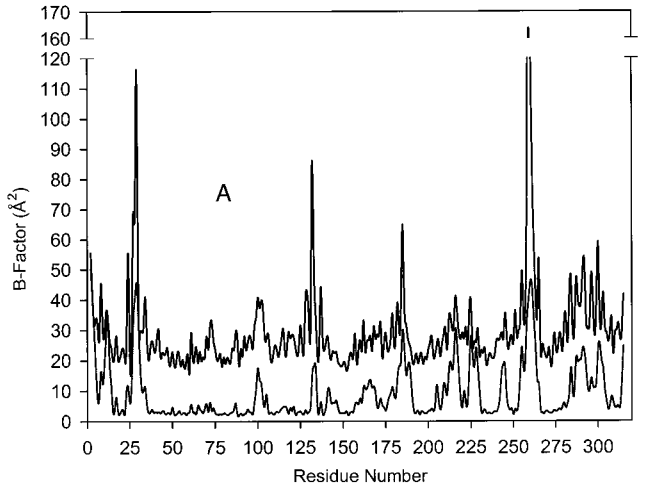

FIGURE 3: Plot of the *B*-factors of the wild type (grey spline) and the Glu105Lys mutant form (black spline). *B*-factors were averaged from all six NCS-related copies. The mutant *B*-factors are, on a per residue basis, approximately 20 Å^2 higher than the wild-type structure except in the calcium-binding site regions which have higher disorder.

its structure. The presence of the hexamer in a new crystal form along with its surprising intermolecular interaction provides additional support for the idea that the hexamer has a biological function, albeit as yet unknown.

Proposed Mechanism for Hexamerization in the E105K Mutant. In the wild-type structure, the intermolecular Ca^{2+} balances the negative Glu105 carboxylate and DE-loop carbonyl oxygens and negative Glu76 carboxylate from helix E. Aside from lacking calcium, the mutant protein was crystallized at pH 5.6 where protonation states of ionizable groups differ from those in the wild-type pH 7.8 structure. Glu76, being hydrogen-bonded to the respective hydrogen bond donor/acceptor of the Thr103 backbone, must be protonated to adopt such an interaction. The wild-type structure lacks this latter feature. In this model, the Glu76 pK_a would have to be elevated by 2−2.5 pH units in order to retain a proton at this pH. Furthermore, as Glu76 is pushed away from the E105K region, it becomes buried and energetically unfavorable for it to be charged rather than protonated. As seen in Figure 5, the E105K region is composed of numerous intermolecular hydrogen bonds formed between Lys105 and surrounding oxygens as well as a tandem hydrogen bond interaction between Glu76 of one molecule and Thr103 of another molecule. We propose that these new interactions can offset hexamer destabilization caused by the loss of calcium binding in the conditions described here. As previously studied, neither chemical cross-linking (*20*) nor small-angle X-ray scattering (SAXS, unpublished data) show the presence of E105K hexamers at pH 7.4 and 7.7, respectively, but do so for the wild-type protein. However, SAXS shows hexamerization to be maximal at pH 5.0 in a calcium-*independent* fashion. Because other ionizable intermolecular interactions are unchanged, the Glu76-*COOH* to Thr103-*C*═*O* hydrogen bond is the most likely candidate for a pH-*dependent* hexamerization switch. With Glu76 protonated at pH 5.6, an increase in pH would deprotonate the carboxylic acid OE2, thus dissociating the hydrogen bond with the Thr103 carbonyl oxygen as shown in Figure 6.

DISCUSSION

Setting out to disrupt the electrostatic balance of the intermolecular calcium-binding site by replacing the wild-type conserved glutamate with lysine at position 105, we expected the mutation to prevent intermolecular calcium-binding and hexamerization. Contrary to our expectations, the mutation stabilizes the hexamer under the crystallization conditions used here.

The ϵ-amino group of Glu105Lys is nearly superimposable with the original intermolecular calcium position, at first suggesting that it takes the role of calcium in hexamerization. However, the hydrogen bonds between the Lys105 ϵ-amino group, the Asp230 carboxylate, and the DE-loop carbonyl oxygens do not suffice for hexamerization. Upon protonation, the new Glu76-*COOH*−Thr103-*C*═*O* hydrogen bond appears to be responsible for pH-dependent hexamerization. Repeated 6 times in the hexamer, each bond contributes 0.5−1.5 kJ/mol, and if lost upon increase of pH or addition of calcium, would account for a substantial destabilization contributing to hexamer breakdown. Aside from the electrostatic and steric complimentarity at the trimer−trimer interface, the balance for hexamer formation relies on this intermolecular site to provide the interactions needed for stability, whether it is in the mutant or wild-type structure. Initially, the presence of the hexamer was thought to be an artifact of crystal-packing forces. A rigorous analysis of crystal-packing contacts in both the wild-type and mutant structures revealed that these are essentially identical between the concave sides of the hexamer but not between side-to-side inter-hexameric interactions. Conservation of these contacts between the two crystal forms is indicative of the preference of the protein for face-to-face stacking of individual trimers. An alternate hexamer could be envisioned as containing the trimers complexed at their concave sides, allowing the calcium/phospholipid-binding sites to be fully accessible for membrane aggregation and possibly fusion as shown in Figure 2. The crystal contacts of this trimer−trimer interface are indeed conserved, but there is very little buried surface reminiscent of protein−protein binding sites. However, it is believed that annexins "flatten" upon membrane binding, allowing all the Ca^{2+}/phospholipid-binding sites to come within close contact to the bilayer (*37*). If so, the contacts between an alternate hexamer might increase and allow for two trimers, each bound to a different bilayer, to form a tight complex bringing these close together as one might expect for vesicular aggregation/fusion events. Cryo-electron microscopy has shown that annexins I and II aggregate membranes by a mechanism where each annexin molecule interacts with one bilayer by its convex face and with the other annexin via its N-terminal concave face forming intermembrane protein junctions (*15*). The distance between the centers of the phospholipid headgroups, and thereby the measurement of this protein-mediated junction, of the two outer leaflets is 80 Å for annexin I and 81 Å for annexin II. In light of this, and with our annexin XII crystallographic hexamers displaying a thickness of 70 Å, the alternate hexamer is an attractive candidate for the form of the protein at this junction.

Oligomerization via a virtually identical pH-dependent switch previously has been described for human thioredoxin (*1*). Human thioredoxin is normally functional as a monomer

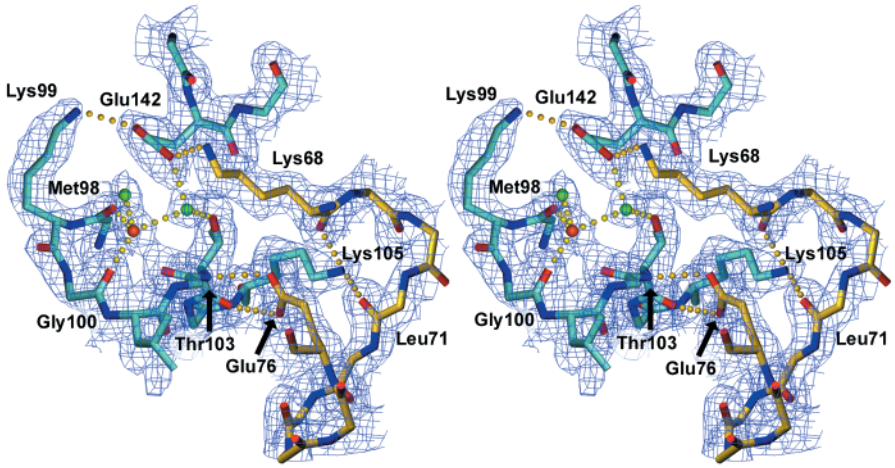

FIGURE 4: Stereoview of the domain II AB-loop binding calcium site where the Glu142 capping residue is involved in two salt-bridges with the loop Lys99 side chain and the Lys68 of the adjacent monomer. This causes the Glu142 side chain to face away from the AB-loop, yet partial occupancy of calcium (orange) in all six AB-loops is observed despite the absence of a capping residue. The Lys99 side chain is more flexible than Lys68, indicating that hexamer formation, donating Lys68 from the adjacent trimers, prevents proper orientation of Glu142 for optimal calcium binding. Water ligands are shown in green. The $2F_o - F_c$ electron density maps are contoured at 1σ. Figure made with Molscript and Raster3D.

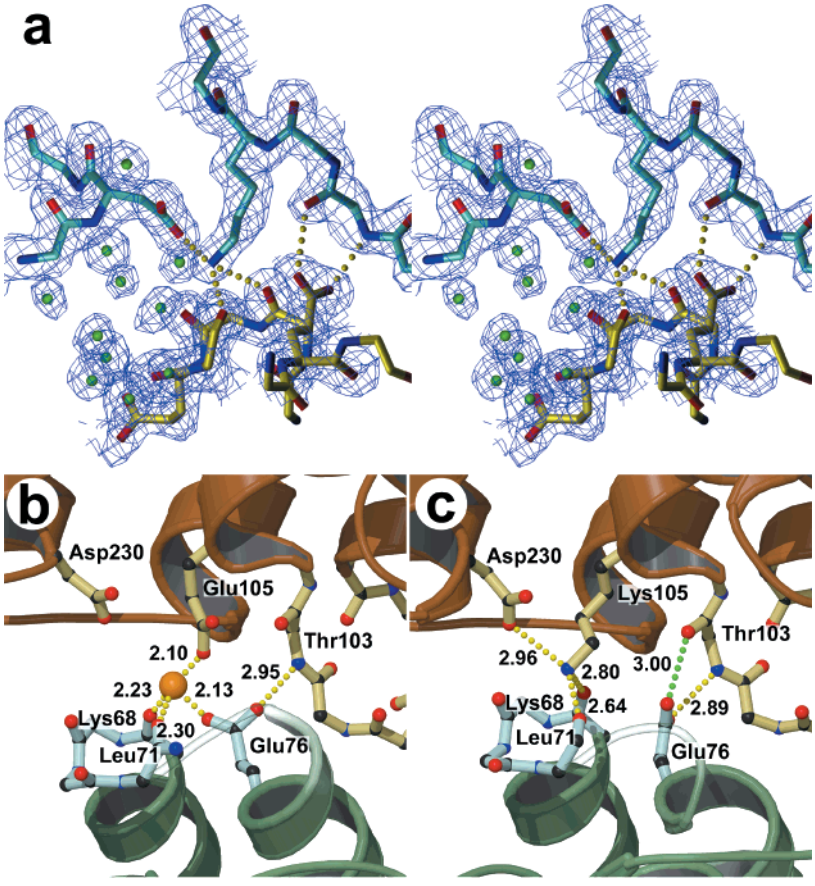

FIGURE 5: View of the E105K mutation site. (a) A stereoplot of a $2F_o - F_c$ electron density map in blue, contoured at 1.0σ, shows the quality of the model in the area of the E105K mutation. The Lys105 side chain fits comfortably in the overall negatively charged area of the DE-loop while Glu76 is itself mostly buried and hydrogen-bonded to the Thr103 peptide backbone. A cluster of water molecules is seen close to this region; these are shown as green spheres. Also shown is the overall difference in ligand coordination and hydrogen bonding between (b) the wild-type structure and (c) the mutant structure. It is evident that Glu76 rotates to form a new hydrogen bond (green). Setor (*8*) was used for (a) and Molscript/Raster3D for (b) and (c).

(reviewed by *11*) but has been shown to exist as inactive homodimers, with their active site buried at the dimer interface (*38*). It was proposed that the possible role of such an inactive form is a mechanism for sensing oxidative stress in tissues or a protective mechanism for the active site of the protein during secretion (*1*, *38*). As shown in subsequent experiments, the interaction occurs pH-dependently via an aspartic acid residue at the dimer interface with an elevated pK_a of 6.5 (*1*). Mutation of this residue to asparagine revealed a pH-independent dimer, in solution and crystallographically, nearly identical to the wild-type thioredoxin, implicating the proposed aspartate/aspartic acid switch in dimerization. We

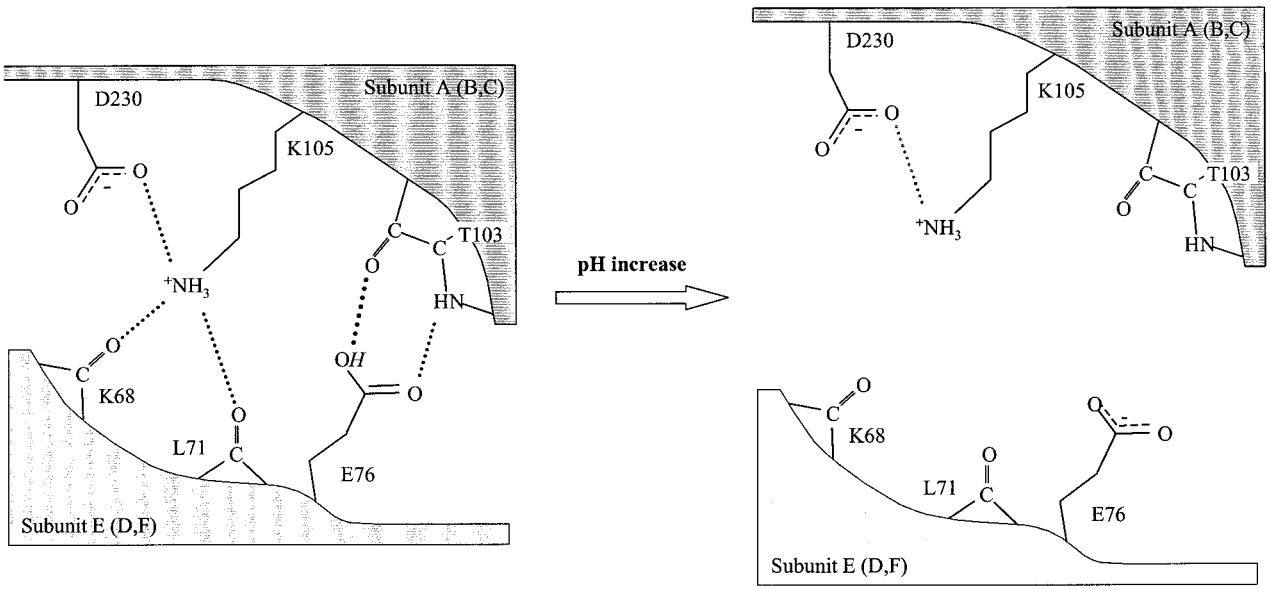

FIGURE 6: Illustration of the pH-dependent switch model for the mutant annexin XII. The Glu105Lys mutation, occurring 6 times throughout the hexamer, is represented here. The dimer pairs are AE, BD, and CF as indicated. At the pH of crystallization, the lysine ϵ-amino group is hydrogen-bonded to the DE-loop carbonyl oxygens, and Glu76 forms two hydrogen bonds with the Thr103 backbone. The protonated state of Glu76-*COOH* stabilizes the hexamer formation. Increasing the pH would cause deprotonation, causing each of the six sites to lose their bond to Thr103-*C═O*. The resulting buried charge would destabilize the hexamer assembly and therefore dissociate the hexamer as shown. It is worth noting that Glu76 in the dissociated state would be amenable to form a type III bidentate ligand to the now free DE-loop carbonyls.

would predict a similar outcome if we were to mutate the annexin XII E105K mutant additionally Glu76 to Gln, one where the pH-dependent hydrogen bond between Glu76 and Thr103 would be replaced by a pH-independent hydrogen bond between the glutamine side chain amide group. The idea that annexin XII may be forming a hexamer as shown here and in the wild-type form may indicate a process in which the protein nearly buries its calcium-binding sites as a means of functional self-regulation. The affinity of the domain II site (unoccupied in the wild-type structure, partially occupied in the E105K structure) may be similar to that in annexin IV, where mutation of the second domain calcium site has a more dramatic effect on membrane aggregation than on binding (*22*). Therefore, hexamerization may control the aggregation properties of wild-type annexin XII by preventing domain II calcium binding. Compared to the trimeric form, the hexamer peripheral type II calcium-binding sites are less accessible to membrane binding, but upon doing so may have a synergistic effect allowing increased membrane binding and hexamer dissociation as the domain II type II site would be freed for calcium and phospholipid binding. The equilibrium of multimeric states, based on the ratio between membrane-bound and free annexin, would also influence the rate of membrane binding in addition to local calcium concentrations and other factors such as phosphorylation.

We observed that addition of calcium to the mutant crystals breaks up their crystal lattice. A possible mechanism is that calcium not only floods the peripheral type II calcium-binding sites but also returns to the intermolecular binding site where it encounters the bulky positively charged lysine, repulses it, and therefore destabilizes the hexamer intermolecular interface. As the two trimers begin to dissociate upon calcium binding to the DE-loop carbonyl oxygens, Glu76 would become solvent-exposed and lose its proton, becoming a calcium ligand forming a true type III site.

The mutation caused local perturbations and led to calcium occupying the domain II AB-loop, which was not observed in the wild-type structure. The domain II capping residue, Glu142, forms salt-bridges with both Lys99 from the same monomer and Lys68 from the opposing monomer. The Lys68 side chain binding at the intermolecular hexamerization site does not appear to veer substantially from its wild-type position. However, the domain II AB-loop-conserved Thr103 attains new interactions with Glu76 of the adjoining monomer. These interactions might be responsible for a slight but significant rearrangement of the AB-loop allowing it to bind calcium, even if weakly, as shown. Physiologically, the loss of this salt-bridge upon trimeric binding to the membrane would liberate the Glu142 and allow it to sequester calcium into the type II calcium-binding site. If present in vivo, this hexameric bridge may act as a mechanism for regulating the amount of calcium bound to the protein and therefore affect membrane-binding affinity.

A similar account has been observed in the *Naja naja naja* phospholipase A_2 where it is proposed that binding of calcium, not in the cofactor site but in the catalytic site, might disrupt the inactive trimer, allowing it to bind phospholipid headgroups (*9*). More recently, *N. naja naja* phospholipase A_2 was crystallized in two novel crystal forms which also formed trimers, now believed to be a unique feature of the *N. naja naja* enzyme (*29*). Interestingly, the calcium-free form shows a calcium-binding glycine-rich loop with an arginine side chain $\eta 1$ nitrogen atom positioned in the proposed second Ca^{2+}-binding site (*9*, *29*). It is believed that Ca^{2+} binding at this second site would cause a conformational change in the arginine side chain and allow the glycine loop to rearrange itself, allowing cofactor Ca^{2+} binding. Furthermore, the catalytic pocket created by the arginine movement is believed to be the site of phospholipid headgroup binding. Under the right physiological conditions, calcium binding in the domain II AB-loop might in fact cause Lys68 motions

large enough to disrupt the intermolecular calcium-binding site it is a part of through its position in the DE-loop, therefore causing hexamer dissociation.

Annexin XII may exhibit such uniqueness in its ability to adopt a plethora of multimeric states, allowing them to adapt to cellular stimuli. Further characterization of the various oligomeric states of annexin XII is under way using a variety of techniques including analytical size-exclusion chromatography, dynamic light scattering, small-angle X-ray scattering (manuscript in preparation), and additional EPR in light of current hypotheses. In vivo characterization will prove to be the most difficult yet the most rewarding.

ACKNOWLEDGMENT

We thank Dr. G. Sheldrick for advice on SHELXH compilation problems, and J. Tran, Dr. A. Rosengarth, and Dr. T. L. Poulos for discussions and critical reading.

REFERENCES

1. Andersen, J. F., Sanders, D. A., Gasdaska, J. R., Weichsel, A., Powis, G., and Montfort, W. R. (1997) *Biochemistry 36*, 13979−13988.
2. Brunger, A. T., Kuriyan, J., and Karplus, M. (1987) *Science 235*, 458−460.
3. Concha, N. O., Head, J. F., Kaetzel, M. A., Dedman, J. R., and Seaton, B. A. (1992) *FEBS Lett. 314*, 159−162.
4. Concha, N. O., Head, J. F., Kaetzel, M. A., Dedman, J. R., and Seaton, B. A. (1993) *Science 261*, 1321−1324.
5. Creutz, C. E., Pazoles, C. J., and Pollard, H. B. (1979) *J. Biol. Chem. 254*, 553−558.
6. Dübel, S. (1989) *Differentiation. 41*, 99−109.
7. Esnouf, R. M. (1997) *J. Mol. Graphics Modell. 15*, 132−134, 112−113.
8. Evans, S. V. (1993) *J. Mol. Graphics 11*, 134−138, 127−128.
9. Fremont, D. H., Anderson, D. H., Wilson, I. A., Dennis, E. A., and Xuong, N. H. (1993) *Proc. Natl. Acad. Sci. U.S.A. 90*, 342−346.
10. Gerke, V., and Moss S. E. (1997) *Biochim. Biophys. Acta 1357*, 129−154.
11. Holmgren, A. (1995) *Structure 3*, 239−243.
12. Huber, R., Romisch, J., and Paques, E. P. (1990) *EMBO J. 9*, 3867−3874.
13. Jones, T. A., Zou, J. Y., Cowan, S., and Kjeldgaard, M. (1991) *Acta Crystallograph. 47*, 110−119.
14. Kleywegt, G. J. (1992−1999) Uppsala University, Uppsala, Sweden, unpublished program.
15. Lambert, O., Gerke, V., Bader, M. F., Porte, F., and Brisson, A. (1997) *J. Mol. Biol. 272*, 42−55.
16. Langen, R., Isas, J. M., Luecke, H., Haigler, H. T., and Hubbell, W. L. (1998) *J. Biol. Chem. 273*, 22453−22457.
17. Laskowski, R. A., MacArthur, M. W., Moss, D. S., and Thornton, J. M. (1993) *J. Appl. Crystallogr. 26*, 283.
18. Liemann, S., Bringemeier, I., Benz, J., Gottig, O., Hofmann, A., Huber, R., Noegel, A. A., and Jacob, U. (1997) *J. Mol. Biol. 270*, 79−88.
19. Luecke, H., Chang, B. T., Maillard, W. S., Schlaepfer, D. D., and Haigler, H. T. (1995) *Nature 378*, 512−515.
20. Mailliard, W. S., Luecke, H., and Haigler, H. T. (1997) *Biochemistry 36*, 9045−9050.
21. Merritt, E. A., and Bacon, D. J. (1997) *Methods Enzymol. 277*, 505−524.
22. Nelson, M. R., and Creutz, C. E. (1995) *Biochemistry 34*, 3121−3132.
23. Otwinowski, Z., and Minor, W. (1996) *Methods Enzymol. 276*.
24. Pepinsky, R. B., Tizard, R., Mattaliano, R. J., Sinclair, L. K., Miller, G. T., Browning, J. L., Chow, E. P., Burne, C., Huang, K. S., and Pratt, D. (1988) *J. Biol. Chem. 263*, 10799.
25. Rothhut, B. (1997) *Cell. Mol. Life Sci. 53*, 522−526.
26. Schlaepfer, D. D., Bode, H. R., and Haigler, H. T. (1992) *J. Cell Biol. 118*, 911−928.
27. Schlaepfer, D. D., Fischer, D. A., Brandt, M. E., Bode, H. R., Jones, J., and Haigler, H. T. (1992b) *J. Biol. Chem. 267*, 9529−9539.
28. Seaton, B. A., Ed. (1996) in *Annexins: molecular structure to cellular function*, R. G. Landes Co., Austin, TX, distributed by Chapman and Hall, New York.
29. Segelke, B. W., Nguyen, D., Chee, R., Xuong, N. H., Dennis, E. A. (1998) *J. Mol. Biol. 279*, 223−232.
30. Sheldrick, G. M., and Schneider, T. (1997) *Methods Enzymol. 277*, 319−343.
31. Sopkova, J., Renouard, M., and Lewit-Bentley, A. (1993) *J. Mol. Biol. 234*, 816−825.
32. Swairjo, M. A., Concha, N. O., Kaetzel, M. A., Dedman, J. R., and Seaton, B. A. (1995) *Nat. Struct. Biol. 2*, 968−974.
33. Swairjo, M. A., and Seaton, B. A. (1994) *Annu. Rev. Biophys. Biomol. Struct. 23*,193−213.
34. Turk, D. (1992) Weiterentwicklung eines Programms fuer Molekuelgraphik und Elektronendichte-Manipulation und seine Anwendung auf verschiedene Protein-Strukturaufklaerungen. Ph.D. Thesis, Technische Universitaet, Muenchen.
35. Turk, D. (1996) Proceedings from the 1996 meeting of the International Union of Crystallography Macromolecular Macromolecular Computing School (Bourne, P. E., and Watenpaugh, K., Eds.) Western Washington University, Bellingham, WA.
36. Weng, X. W., Luecke, H., Song, I., Kang, D. S., Kim, S. H., and Huber, R. (1993) *Protein Sci. 2*, 448−458.
37. Voges, D., Berendes, R., Burger, A., Demange, P., Baumeister, W., and Huber, R. (1994) *J. Mol. Biol. 238*, 199−213.
38. Weichsel, A., Gasdaska, J. R., Powis, G., Montfort, W. R. (1996) *Structure 4*, 735−751.

BI992278D